Element-specific density of states of Co₂MnGe revealed by resonant photoelectron spectroscopy

Takashi Kono ¹, * Masaaki Kakoki, ¹ Tomoki Yoshikawa, ¹ Xiaoxiao Wang, ¹ Kazuki Sumida, ¹, ² Koji Miyamoto, ³ Takayuki Muro, ⁴ Yukiharu Takeda, ⁵ Yuji Saitoh, ⁵ Kazuki Goto, ⁶ Yuya Sakuraba ¹, ⁶ Kazuhiro Hono, ⁶ and Akio Kimura ¹Department of Physical Sciences, Graduate School of Science, Hiroshima University, 1-3-1 Kagamiyama, Higashi-hiroshima 739-8526, Japan

²Department of Physics, Tokyo Institute of Technology, Tokyo 152-8551, Japan

³Hiroshima Synchrotron Radiation Center, Hiroshima University, 2-313 Kagamiyama, Higashi-hiroshima 739-0046, Japan

⁴Japan Synchrotron Radiation Research Institute (JASRI), 1-1-1 Kouto, Sayo, Hyogo 679-5198, Japan

⁵Materials Sciences Research Center, Japan Atomic Energy Agency, Hyogo 679-5148, Japan

⁶National Institute for Materials Science, Sengen 1-2-1, Tsukuba 305-0047, Japan



(Received 24 July 2019; published 14 October 2019)

Resonant photoelectron spectroscopy at the Co and Mn 2p core absorption edges of half-metallic Co₂MnGe has been performed to determine the element-specific density of states (DOS). A significant contribution of the Mn 3d partial DOS near the Fermi level (E_F) was clarified by measurement at the Mn 2p absorption edge. Further analysis by first-principles calculation revealed that it has t_{2g} symmetry, which must be responsible for the electrical conductivity along the line perpendicular to the film plane. The dominant normal Auger contribution observed at the Co 2p absorption edge indicates delocalization of photoexcited Co 3d electrons. The difference in the degrees of localization of the Mn 3d and Co 3d electrons in Co₂MnGe is explained by the first-principles calculation. Our findings of the element-/orbital-specific electronic states near E_F will pave the way for future interface design of magnetic tunneling junctions to overcome the temperature-induced reduction of the magnetoresistance.

DOI: 10.1103/PhysRevB.100.165120

I. INTRODUCTION

After the first prediction in one of the Heusler alloys, NiMnSb [1], a half-metallic electronic structure, in which the majority spin (minority spin) part of the density of states (DOS) is metallic (semiconducting), resulting in 100% spin polarization at the Fermi level (*E*_F), is considered to be the key factor in realizing extremely high magnetoresistance (MR) [2]. First-principles calculations predict that some of the ferromagnetic full-Heusler alloys including Co₂MnGe and Co₂MnSi possess a half-metallic electronic structure [3–5]. These half-metallic full-Heusler alloys, which are more structurally stable than the half-Heusler alloys, are promising for practical application in very elevated MR to tunneling MR (TMR) and current-perpendicular-to-plane giant magnetoresistance (CPP-GMR) devices.

Previous studies of the magnetic tunneling junctions (MTJs) with half-metallic Heusler alloys, such as Co₂MnSi and Co₂MnGe, have shown large TMR ratios reflecting their high spin polarization at low temperature [6–10]. The highest MR ratios of about 1995% and 2610% at 4.2 K have been reported in MTJs using Co₂MnSi and Co₂(Fe,Mn)Si electrodes with a MgO barrier, respectively, which are about twice as large as that of a CoFeB/MgO/CoFeB MTJ with non-half-metallic CoFeB layers [11]. However, the high TMR ratio in half-metallic Heusler-based MTJs sharply decreases with

increasing temperature. It is considered that the interfacial problems between the Heusler electrode and the tunneling barrier, such as formation of an interfacial in-gap state [12,13] and reduction of the interfacial exchange stiffness [14–18], are important factors in determining the TMR ratio at room temperature. High MR ratios arising from high spin polarization of Co₂MnSi and Co₂MnGe have also been reported for CPP-GMR devices [19,20]. In both MTJs and CPP-GMR using half-metallic Heusler electrodes, interfacial electronic band matching with the tunneling barrier or metallic spacer is a crucial factor that determines the magnitude of the MR ratio [21-23]. Therefore, it is necessary to control the interfacial electronic and magnetic states that contribute to spin-dependent transport through the interface. As a first step, the bulk electronic structure of the half-metallic Heusler layer that governs the MR ratio must be investigated in detail.

Photoelectron spectroscopy (PES) is one of the most powerful tools for directly observing the electronic band structures of solids. Numerous studies have probed the valence band DOS of Co_2Mn -based Heusler alloys with vacuum ultraviolet radiation [24,25] and hard x rays [14,24,26–28]. However, previous studies showed that PES was generated from the element-unresolved DOS under E_F , although the element-resolved information of the band is important to understand coherent transport through the crystalline tunneling barrier, such as MgO [21]. Resonant PES (RPES) in core excitation regions enables the DOS to be resolved in an element-specific way [29]. RPES in the Mn and Co 3p-3d core absorption regions of Co_2MnSn has been performed [30]. However,

^{*}takashi-kono@hiroshima-u.ac.jp

[†]akiok@hiroshima-u.ac.jp

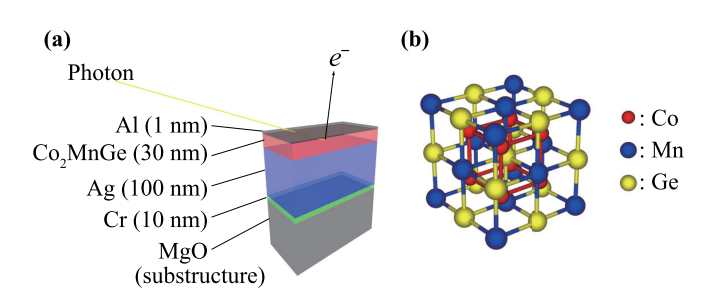


FIG. 1. (a) Composition of the film. The electrons of the sample layer pass through the Al cap layer and are emitted into the vacuum. (b) Crystal structure of Co₂MnGe.

complicated interference effects including the Fano effect, and the greatly enhanced surface sensitivity of the RPES in the vacuum ultraviolet region prevented the measurement from obtaining the correct electronic structure of the buried bulk and interface DOS. RPES with a deeper escape depth of photoelectrons using soft x-ray synchrotron radiation in the transition metal 2p core absorption region has not been performed, even for prototypical full-Heusler alloys such as Co₂MnSi and Co₂MnGe. Among the various half-metallic Co-based Heusler alloys, Co₂MnGe is one of the most promising materials for practical applications because high atomic ordering can be obtained in Co₂MnGe at low annealing temperature [20]. In this study, we determined the element-/ orbital-resolved electronic structures of Co₂MnGe by soft x-ray PES in the Mn and Co 2p-3d core excitation regions with sufficient bulk sensitivity. The obtained valence band spectra were compared with the theoretical PDOS obtained by a first-principles calculation.

II. EXPERIMENTAL

The RPES experiments were performed at the BL25SU soft x-ray beamline of SPring-8. The energy resolution was estimated to be full width at half maximum (FWHM) of 80 meV by the Fermi cutoff of deposited gold films. The x-ray absorption spectroscopy (XAS) experiments were performed at BL23SU of SPring-8 using the total electron yield method [31]. All of the measurements were performed about 40 K.

A thin film sample of Co_2MnGe was prepared by the magnetron sputtering method at the National Institute for Materials Science. A 30-nm-thick Co_2MnGe film was grown by Ar^+ ion sputtering of the polycrystalline target onto a MgO substrate with buffer layers of Cr (10 nm) and Ag (100 nm) to suppress the surface roughness [Fig. 1(a)]. Finally, the sample was capped with Al (1 nm) to prevent the surface from further oxidation. X-ray diffraction and x-ray fluorescence measurements confirmed the $L2_1$ ordered phase of the film.

We also performed first-principles density-functional calculations with the WIEN2K program [32]. We used the spin-polarized generalized gradient approximation [33]. Coulomb interaction U is not considered here because previous studies show that U does not affect its electronic structure [34,35].

The muffin-tin approximation was used for the potential, and the muffin-tin radius $R_{\rm MT}$ of each atom was taken to be $R_{\rm MT}^{\rm Co}=R_{\rm MT}^{\rm Mn}=2.30$ Bohr and $R_{\rm MT}^{\rm Ge}=2.23$ Bohr. The wave functions were expanded by spherical harmonics with ℓ to $\ell_{\rm max}=10$ in the muffin-tin spheres and by plane waves in the interstitial region with a cutoff value of $R_{\rm MT}^{\rm Ge} \cdot K_{\rm max}=7$. The Fourier charge density was expanded up to $G_{\rm max}=12\,{\rm Bohr}^{-1}$. The k space was divided into a uniform $21\times21\times21$ mesh. These $RK_{\rm max}$, $\ell_{\rm max}$, $G_{\rm max}$, and k points were sufficient to stabilize the shape of DOS. We assumed that the lattice constants were $a=b=c=5.700\,{\rm \AA}$ and $\alpha=\beta=\gamma=90^\circ$ (theoretical value [36]) in this calculation. The space group of ${\rm Co}_2{\rm MnGe}$ was $Fm\bar{3}m$. We set the atomic positions as Co (0.25,0.25,0.25), Mn (0,0,0), and Ge (0.5,0.5,0.5) [Fig. 1(b)].

III. RESULTS AND DISCUSSION

We performed RPES in the Mn 2p-3d core absorption region ($h\nu = 634-642$ eV). The Mn 2p-3d XAS spectrum is shown in Fig. 2(a). The absorption maximum is at $h\nu =$ 639.5 eV with some fine structures. Note that these multiplet structures are slightly sharper than in a previously reported spectrum of bulk Co₂MnGe [37,38]. This is probably because of the presence of partially oxidized Mn at the interface with the Al capping layer. The excitation energies used for the RPES spectra are labeled on the Mn 2p-3d XAS spectrum [Fig. 2(a)]. The valence band spectra were normalized by the sum of the Ge $3d_{5/2}$ and $3d_{3/2}$ photoelectron intensities (not shown), which does not contribute to the resonance process. The valence band spectra in Fig. 2(b) show that there is no significant change with the incident photon energy $h\nu$ below the absorption edge (see spectra 1–3). Here, spectrum 1 is regarded as a nonresonant (normal) PES spectrum. A large increase in the intensity is observed at the Mn 2p absorption

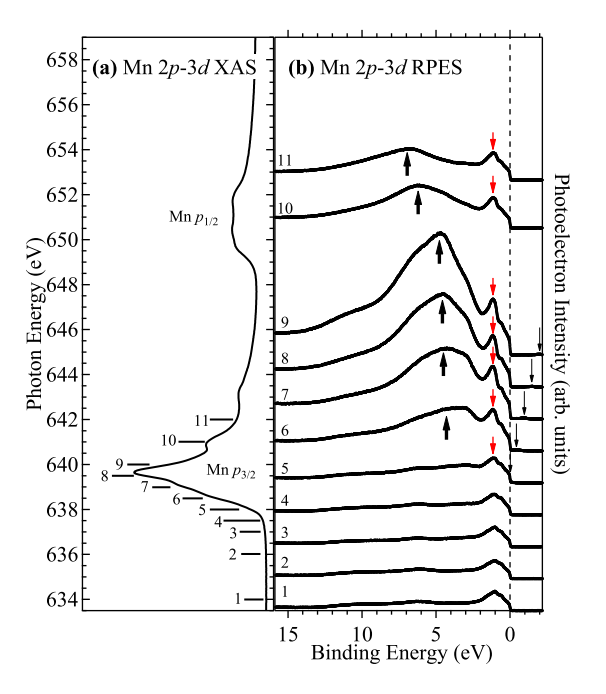


FIG. 2. (a) Mn L_{23} XAS spectrum. (b) Valence band PES spectra in Mn 2p-3d core absorption region. Labels 1–11 denote excitation energies that correspond to those in (a).

edge (spectra 6-9). Enhancement of the Mn 3d component is expected by the resonant photoelectron process described by Mn $2p^6 3d^n \to 2p^5 3d^{n+1} \to 2p^6 3d^{n-1} + e^-$. It should be noted that intensity enhancement can also occur by the normal Auger process described by Mn $2p^63d^n \rightarrow 2p^53d^{n+1} \rightarrow$ $2p^63d^{n-2} + e^-$. The normal Auger peak linearly shifts to higher binding energy $(E_{\rm B})$ with increasing $h\nu$, while the resonance peak stays at the same $E_{\rm B}$ independent of $h\nu$. Marked enhancement can be observed in spectra 6-9 because $E_{\rm B}$ of the normal Auger peaks shifts away from $E_{\rm F}$ [thick arrows in Fig. 2(b)]. However, closer inspection of spectra 4–9 shows that the intensity around $E_{\rm B}=1~{\rm eV}$ is enhanced without any shift of E_B [red arrows in Fig. 2(b)], indicating the resonant origin of this feature. In addition, spectra 5–9 are accompanied by small peaks that linearly shift to lower $E_{\rm B}$ with increasing $h\nu$ (thin arrows). This is ascribed to the Ge 2p core level photoelectron signal caused by the second-order light from the monochromator.

First, we compare the nonresonant PES spectrum [spectrum 1, Fig. 3(a)] with the theoretical PES spectrum constructed from the calculated PDOS multiplied by the Fermi-Dirac distribution function and convoluted with a Gaussian function considering the energy resolution of FWHM ~ 80 meV [Fig. 3(b)]. The PDOSs in Fig. 3(b) are weighted by the photoionization cross section [39]. In the experimental nonresonant spectrum in Fig. 3(a), the prominent peak N2 is located at $E_{\rm B}\sim 1~{\rm eV}$ and the shoulder structure N1 is close to the E_F . In the calculated spectrum [Fig. 3(b)], the β peak at $E_{\rm B}\sim 1$ eV and shoulder structure α appear. When the calculated DOS shifts to higher $E_{\rm B}$ by 135 meV, the energy positions of these structures match the experimental results. Other structures at higher $E_{\rm B}$ than structure β are not very visible in the theoretical DOS. These structures might be hindered by secondary electrons and could also be obscured because of energy-dependent lifetime broadening. In the RPES spectrum [spectrum 7, Fig. 3(a)], structures R1 and R2 that are similar to structures N1 and N2 in the nonresonant spectrum are observed. Furthermore, a broad feature is observed at about $E_{\rm B}=5$ eV. These are ascribed to the Mn 3d component because they are enhanced by the Mn 2p-3d resonance process.

The difference spectrum was produced by subtracting the nonresonant spectrum taken before the absorption edge from the resonant spectrum [Fig. 3(c)]. The calculated Mn 3dPDOS with an energy offset of 135 meV toward higher $E_{\rm B}$ is shown in Fig. 3(d). The calculated PDOS was multiplied by the Fermi-Dirac distribution function, as for the simulated DOS in Fig. 3(b), and convoluted with the Gaussian function considering the energy resolution of the difference spectrum (FWHM ~ 80 meV). The Mn 3d PDOS was further decomposed into e_g and t_{2g} components [Fig. 3(d)]. It can again be safely stated that shoulder structure D1 and peak D2 correspond to α and β of the calculated Mn 3d PDOS, respectively. The observed peak D3 coincides with the theoretical peak γ with Mn 3d t_{2g} character. The height of the peak D3 in the experimental result is very large relative to the calculated result, partly because of the contribution from the normal Auger component that cannot be subtracted and also a possible contribution from oxidized Mn at the interface with the Al capping layer. However, it should be emphasized

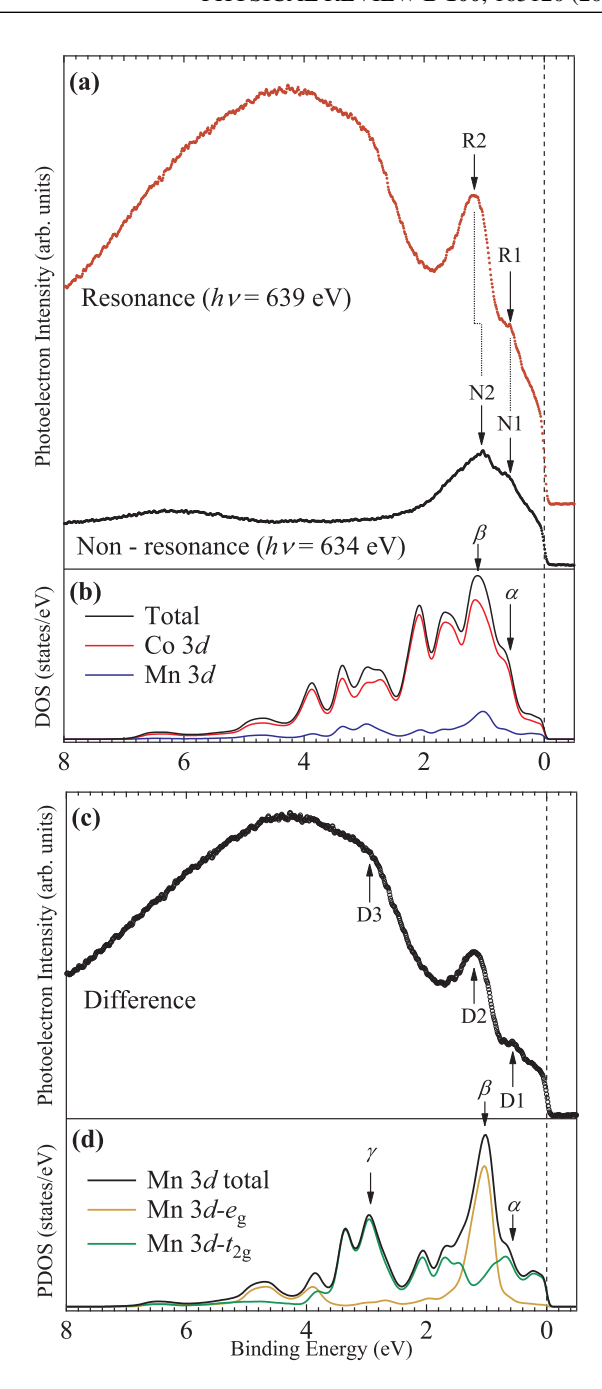


FIG. 3. (a) Nonresonance spectrum [spectrum 1 in Fig. 2(b)] and resonance spectrum [spectrum 7 in Fig. 2(b)]. (b) Theoretical total Co 3d and Mn 3d PDOS obtained by first-principles calculation considering photoionization cross section and resolution with an energy offset of 135 meV toward higher $E_{\rm B}$. (c) Difference spectrum obtained by subtracting spectrum 1 from spectrum 7. (d) Calculated Mn PDOS with its $e_{\rm g}$ and $t_{\rm 2g}$ components.

that these do not affect the DOS near $E_{\rm F}$, which is the main scope of the present study. In fact, bulk band dispersion of GaAs buried under the As capping layer is observed in the excitation energy range from 500 to 1000 eV [40]. From Fig. 3, it can be concluded that the Mn 3d t_{2g} orbital derived state crosses $E_{\rm F}$, while peak D2 in Fig. 3(c) is ascribed to the exchange-split Mn 3d $e_{\rm g}$ state that forms a minority spin gap.

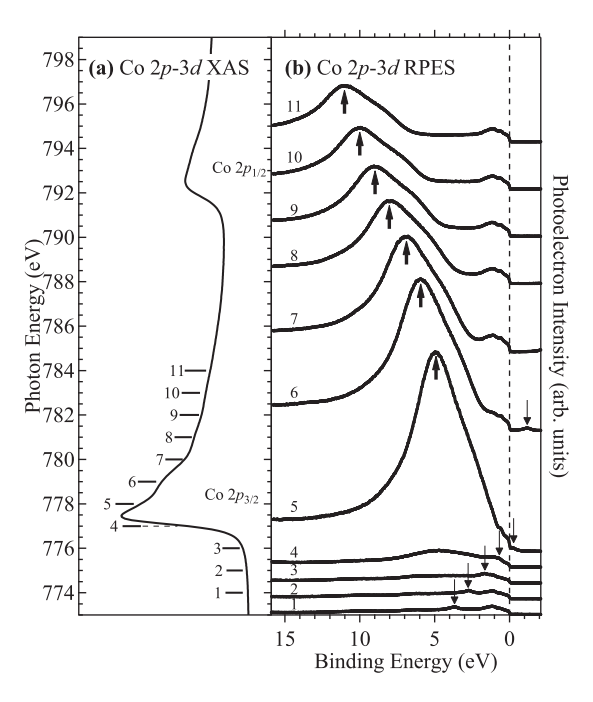


FIG. 4. (a) Co L_{23} XAS spectrum. (b) Valence band PES spectra in Co 2p-3d core absorption region. Labels 1–11 denote excitation energies that correspond to those in (a).

Next, we consider the Co 3d PDOS. To extract the Co 3d PDOS, we performed RPES in the Co 2p-3d core absorption region ($h\nu = 634-642$ eV). The excitation energies required for RPES were obtained from the Co 2p-3d XAS spectra [Fig. 4(a)]. The valence band spectra shown in Fig. 4(b) were normalized in the same way as those for Mn 2p-3d RPES. A large increase in the intensity is observed in spectra 5-11. The intensity maximum of such prominent features linearly shifts to higher $E_{\rm B}$ with increasing $h\nu$ [thick arrows in Fig. 4(b)], indicating that normal Auger emission mainly occurs. In addition, the increase in the intensity with no shift of $E_{\rm B}$ is negligible. We thus conclude that the resonance feature is hardly observed, but the normal Auger process is dominant in the Co 2p-3d absorption region in sharp contrast to the case at the Mn 2p edge. It should be noted that spectra 1–7 exhibit small peaks that linearly shift to lower $E_{\rm B}$ with increasing $h\nu$ (thin arrows). This is ascribed to the Al 1s core level photoelectron signal from the capping layer by the second-order light. This also makes it difficult to extract the Co PDOS by taking spectral differences.

As mentioned above, the normal Auger process dominates by Co 2p-3d core absorption, while the resonant process occurs by Mn 2p-3d core excitation. In RPES, $E_{\rm B}$ constant resonance excitation occurs when the intermediate electronic state in the resonant (final state in core absorption) process is expected to be relatively localized, which leads to direct recombination of photoexcited electrons. Conversely, if the photoexcited 3d electrons are delocalized, excited electrons relax to the other orbital before returning to the inner shell (2p), where direct recombination is largely suppressed [41]. Therefore, the difference in the dominance of the normal Auger process between Mn and Co 2p-3d core absorption can be accounted for in terms of the difference in the degree of localization of photoexcited electrons. The calculated band

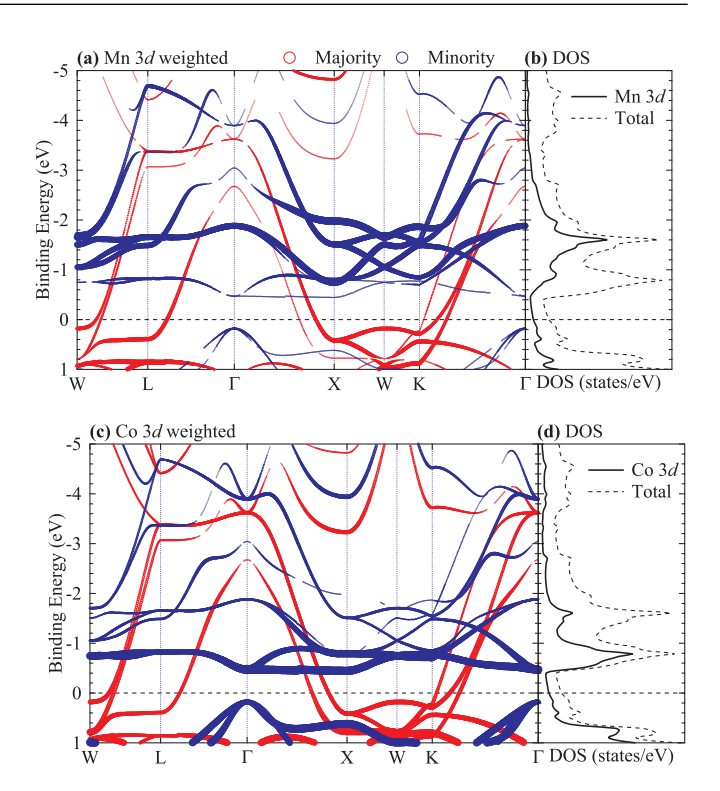


FIG. 5. (a) and (c) Calculated band structures of Co_2MnGe . Red and blue correspond to majority spin and minority spin. Thickness of line shows the weight of (a) Mn 3d and (c) Co 3d orbitals. (b) and (d) Calculated PDOSs of Co_2MnGe . Dashed line donates the total DOS

dispersions weighted by the Mn 3d and Co 3d states are shown in Figs. 5(a) and 5(c), respectively. The corresponding Mn 3d and Co 3d PDOSs are shown in Figs. 5(b) and 5(d). It can be determined that the narrower (wider) band width dictates the more localized (itinerant) feature of the electrons. From Fig. 5, there is a flat dispersion at the upper edge (\sim 0.8 eV above $E_{\rm F}$) of the half-metallic gap. In addition, the other minority spin bands between 1 and 2 eV above E_F are much less steep than the majority spin bands in the same energy range. By comparing the band dispersions in Figs. 5(a) and 5(c), the flat bands in the range 1–2 eV are dominated by the Mn 3d components without significant contributions from the Co 3d states. This indicates that the photoexcited electrons by Mn 2p-3d absorption can be localized at the Mn site and recombine with the created 2p holes, enhancing the resonant photoelectron process. Conversely, the flat bands in the upper edge of the minority spin gap are dominated by the Co 3d states with e_u symmetry [Fig. 5(c)] [5]. This could lead to resonance enhancement near the Co 2p-3d absorption threshold. However, marked intensity enhancement is not observed [see spectrum 4 in Fig. 4(b)]. At 1–3 eV above E_F , where Mn 3d flat bands and dispersive Co 3d bands are present, the photoexcited electrons by Co 2p-3d absorption exhibit strong itinerancy and do not remain at the same atomic site, which triggers normal Auger emission. This has been theoretically shown to explain the localized magnetic moments from the delocalized electron system of Heusler alloys [3]. We believe that the present PES in the Mn and Co 2p-3d core excitation regions experimentally verifies this theoretical scenario.

IV. CONCLUSION

Soft x-ray PES experiment of a Heusler-type Co_2MnGe film in the Mn 2p-3d core excitation region has clarified the significant contribution of Mn 3d electrons to the states near E_F . Further analysis by first-principles calculation revealed that it has t_{2g} symmetry, which must be responsible for the electrical conductivity along the line perpendicular to the film plane. From the dominant normal Auger contribution to the valence band spectra in the Co 2p-3d absorption region, the Co 3d states have more itinerant character than the Mn 3d states 1-3 eV above E_F . In addition, the prohibited resonant Auger process at the onset of Co 2p-3d absorption indicates that the upper edge of the minority spin gap consists of the Co 3d e_u flat band, which is orthogonal to the other Co 3d orbitals below E_F . This is also supported by ab initio calculations. The present findings will greatly assist future

interface design of the MTJs incorporating half-metallic Heusler alloys to overcome the temperature-induced reduction of the magnetoresistance.

ACKNOWLEDGMENTS

This work was supported by JSPS KAKENHI (Grants No. 17H06152 and No. 18H03683). The soft x-ray absorption spectroscopy experiments were performed at SPring-8 under the Shared Use Program of JAEA Facilities with the approval of the Nanotechnology Platform project supported by the Ministry of Education, Culture, Sports, Science and Technology (Proposal No. 2018B3842). The soft x-ray PES experiment was performed with the approval of JASRI (Proposal No. 2018B1019). T.Y. and K.S. were financially supported by Grants-in-Aid for JSPS Fellows No. 18J22309 and No. 19J00858, respectively.

- [1] R. A. de Groot, F. M. Mueller, P. G. vanEngen, and K. H. J. Buschow, Phys. Rev. Lett. 50, 2024 (1983).
- [2] M. Julliere, Phys. Lett. A 54, 225 (1975).
- [3] J. Kübler, A. R. Williams, and C. B. Sommers, Phys. Rev. B 28, 1745 (1983).
- [4] S. Ishida, S. Fujii, S. Kashiwagi, and S. Asano, J. Phys. Soc. Jpn. 64, 2152 (1995).
- [5] I. Galanakis, P. H. Dederichs, and N. Papanikolaou, Phys. Rev. B 66, 174429 (2002).
- [6] Y. Sakuraba, M. Hattori, M. Oogane, Y. Ando, H. Kato, A. Sakuma, T. Miyazaki, and H. Kubota, Appl. Phys. Lett. 88, 192508 (2006).
- [7] S. Tsunegi, Y. Sakuraba, M. Oogane, K. Takanashi, and Y. Ando, Appl. Phys. Lett. 93, 112506 (2008).
- [8] T. Taira, T. Ishikawa, N. Itabashi, K. ichi Matsuda, T. Uemura, and M. Yamamoto, J. Phys. D: Appl. Phys. 42, 084015 (2009).
- [9] H.-X. Liu, Y. Honda, T. Taira, K.-I. Matsuda, M. Arita, T. Uemura, and M. Yamamoto, Appl. Phys. Lett. 101, 132418 (2012).
- [10] K. Moges, Y. Honda, H.-X. Liu, T. Uemura, M. Yamamoto, Y. Miura, and M. Shirai, Phys. Rev. B 93, 134403 (2016).
- [11] S. Ikeda, J. Hayakawa, Y. Ashizawa, Y. M. Lee, K. Miura, H. Hasegawa, M. Tsunoda, F. Matsukura, and H. Ohno, Appl. Phys. Lett. 93, 082508 (2008).
- [12] P. Mavropoulos, M. Ležaić, and S. Blügel, Phys. Rev. B 72, 174428 (2005).
- [13] T. Ishikawa, H. Liu, T. Taira, K.-I. Matsuda, T. Uemura, and M. Yamamoto, Appl. Phys. Lett. 95, 232512 (2009).
- [14] K. Miyamoto, A. Kimura, Y. Miura, M. Shirai, M. Ye, Y. Cui, K. Shimada, H. Namatame, M. Taniguchi, Y. Takeda, Y. Saitoh, E. Ikenaga, S. Ueda, K. Kobayashi, and T. Kanomata, Phys. Rev. B 79, 100405(R) (2009).
- [15] A. Sakuma, Y. Toga, and H. Tsuchiura, J. Appl. Phys. 105, 07C910 (2009).
- [16] Y. Sakuraba, K. Takanashi, Y. Kota, T. Kubota, M. Oogane, A. Sakuma, and Y. Ando, Phys. Rev. B 81, 144422 (2010).
- [17] Y. Miura, K. Abe, and M. Shirai, Phys. Rev. B 83, 214411 (2011).

- [18] S. Tsunegi, Y. Sakuraba, K. Amemiya, M. Sakamaki, E. Ozawa, A. Sakuma, K. Takanashi, and Y. Ando, Phys. Rev. B 85, 180408(R) (2012).
- [19] T. Iwase, Y. Sakuraba, S. Bosu, K. Saito, S. Mitani, and K. Takanashi, Appl. Phys. Exp. 2, 063003 (2009).
- [20] M. J. Carey, S. Maat, S. Chandrashekariaih, J. A. Katine, W. Chen, B. York, and J. Childress, J. Appl. Phys. 109, 093912 (2011).
- [21] Y. Miura, H. Uchida, Y. Oba, K. Abe, and M. Shirai, Phys. Rev. B 78, 064416 (2008).
- [22] Y. Miura, K. Futatsukawa, S. Nakajima, K. Abe, and M. Shirai, Phys. Rev. B 84, 134432 (2011).
- [23] Y. Sakuraba, K. Izumi, T. Iwase, S. Bosu, K. Saito, K. Takanashi, Y. Miura, K. Futatsukawa, K. Abe, and M. Shirai, Phys. Rev. B 82, 094444 (2010).
- [24] M. Jourdan, J. Minár, J. Braun, A. Kronenberg, S. Chadov, B. Balke, A. Gloskovskii, M. Kolbe, H. J. Elmers, G. Schönhense, H. Ebert, C. Felser, and M. Kläui, Nat. Commun. 5, 3974 (2014).
- [25] R. Fetzer, B. Stadtmüller, Y. Ohdaira, H. Naganuma, M. Oogane, Y. Ando, T. Taira, T. Uemura, M. Yamamoto, M. Aeschlimann, and M. Cinchetti, Sci. Rep. 5, 8537 (2015).
- [26] D. Brown, M. D. Crapper, K. H. Bedwell, M. T. Butterfield, S. J. Guilfoyle, A. E. R. Malins, and M. Petty, Phys. Rev. B 57, 1563 (1998).
- [27] S. Ouardi, G. H. Fecher, B. Balke, A. Beleanu, X. Kozina, G. Stryganyuk, C. Felser, W. Klöß, H. Schrader, F. Bernardi, J. Morais, E. Ikenaga, Y. Yamashita, S. Ueda, and K. Kobayashi, Phys. Rev. B 84, 155122 (2011).
- [28] X. Kozina, J. Karel, S. Ouardi, S. Chadov, G. H. Fecher, C. Felser, G. Stryganyuk, B. Balke, T. Ishikawa, T. Uemura, M. Yamamoto, E. Ikenaga, S. Ueda, and K. Kobayashi, Phys. Rev. B 89, 125116 (2014).
- [29] S. Hüfner, Photoelectron Spectroscopy: Principles and Applications, 3rd ed. (Springer, Berlin/Heidelberg, 2003).
- [30] M. Baral, S. Banik, A. Chakrabarti, D. Phase, and T. Ganguli, J. Alloys Compd. 645, 112 (2015).

- [31] Y. Saitoh, Y. Fukuda, Y. Takeda, H. Yamagami, S. Takahashi, Y. Asano, T. Hara, K. Shirasawa, M. Takeuchi, T. Tanaka, and H. Kitamura, J. Synch. Rad. 19, 388 (2012).
- [32] P. Blaha, K. Schwarz, G. K. H. Madsen, D. Kvasnicka, and J. Luitz, WIEN2K, An Augmented Plane Wave + Local Orbitals Program for Calculating Crystal Properties (Karlheinz Schwarz, Techn. Universität Wien, Austria, 2001).
- [33] J. P. Perdew, K. Burke, and M. Ernzerhof, Phys. Rev. Lett. 77, 3865 (1996).
- [34] C. Tsirogiannis and I. Galanakis, J. Magn. Magn. Mater. 393, 297 (2015).
- [35] S. Sharma and S. K. Pandey, J. Magn. Magn. Mater. 403, 1 (2016).

- [36] H. M. Huang, S. J. Luo, and K. L. Yao, Phys. Status Solidi B 249, 840 (2011).
- [37] K. Miyamoto, K. Iori, A. Kimura, T. Xie, M. Taniguchi, S. Qiao, and K. Tsuchiya, Solid State Commun. 128, 163 (2003).
- [38] K. Miyamoto, A. Kimura, K. Iori, K. Sakamoto, T. Xie, T. Moko, S. Qiao, M. Taniguchi, and K. Tsuchiya, J. Phys. Condens. Matter 16, 5797 (2004).
- [39] J. Yeh and I. Lindau, At. Data Nucl. Data Tables 32, 1 (1985).
- [40] M. Kobayashi, I. Muneta, T. Schmitt, L. Patthey, S. Ohya, M. Tanaka, M. Oshima, and V. N. Strocov, Appl. Phys. Lett. 101, 242103 (2012).
- [41] M. Zangrando, E. Magnano, A. Nicolaou, E. Carleschi, and F. Parmigiani, Phys. Rev. B 75, 233402 (2007).